

Multi-mode Sensitive Layout Synthesis of Microresonators

Sitaraman Iyer,[†] Tamal Mukherjee[†] and Gary K. Fedder^{†*}

[†]Department of Electrical and Computer Engineering and ^{*}The Robotics Institute
Carnegie Mellon University
Pittsburgh, PA, 15213-3890

ABSTRACT

Microresonator layouts are synthesized such that their preferred mode of oscillation is well-separated from the higher order in-plane and out-of-plane modes. Building on our previous work, we have incorporated models for four out-of-plane modes. All these modes are modeled as spring-mass systems. The spring constants and the effective masses of these modes are analytically derived. Synthesis is accomplished by encoding a design quality metric as the design objective while simultaneously constraining the design to meet user specifications. These constraints require that the resonant frequency in the preferred direction is sufficiently lower than (and, hence, dominates over) the resonant frequency of other modes of vibration of the structure. The models are verified by comparison with 3D FEM simulations and also with experimental measurements on fabricated resonators. The usefulness of these models is illustrated by comparing the oscillation modes of layouts synthesized with and without these models. This exercise also shows that such mode-separation can be achieved only if the microresonators have a structural thickness larger than flexure width.

Keywords: CAD, resonator, synthesis

INTRODUCTION

Designers of surface micromachined MEMS are showing an increasing demand for CAD tools to aid in rapid design. System-level designers integrating many similar but not identical MEMS devices into sensing and actuation systems, are constrained by the lack of MEMS cell libraries. To overcome this design bottleneck, we have been focusing on a design tool to generate MEMS component layouts from engineering specifications. For our initial example, we have chosen the surface-micromachined MEMS resonator [1], shown in Figure 1. This device is commonly used for process characterization, and is chosen because its behavior is well-understood.

Automatic layout generation allows the MEMS designer to focus on designing new topologies and system-level design issues rather than on sizing individual devices to meet the specifications. Layout generation from user input of physical device dimensions [2][3] and device-level trade-offs for optimality [4] have been reported. Our previous work has demonstrated a full-fledged layout synthesis approach [5]. This approach combines lumped-parameter electromechanical models with optimization for the rapid

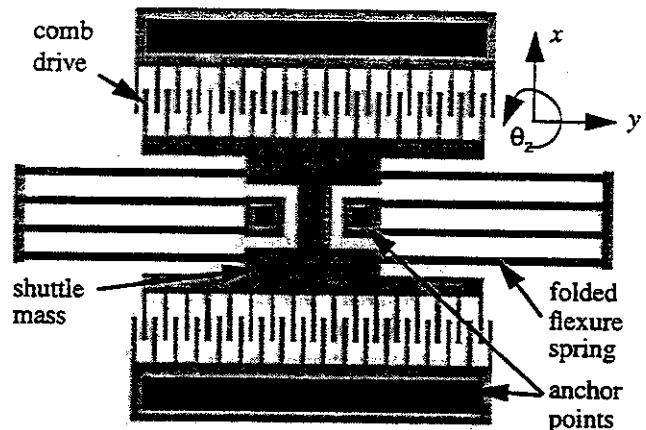


FIGURE 1. Layout of the lateral folded-flexure comb-drive microresonator. The black areas are the places where the polysilicon structure is anchored to the bottom layer. The rest of the structure is suspended 2 μm above the bottom layer.

synthesis of MEMS layout. We now enhance our synthesis tool by incorporating additional models that capture the 3D nature of MEMS devices by considering both out-of-plane and in-plane device behavior. This enables us to synthesize resonators which have well-controlled modes of oscillation. To ensure this, we model the resonator in all its principal modes of oscillation. This lumped-parameter-based approach to synthesis will be a viable source for on-the-fly MEMS cell generation only if the predictions of device performance match actual device performance. The development of accurate models within an arbitrary design space is a difficult problem, which we overcome by ensuring that our models are adequately accurate in the region they expect to be used. Therefore, instead of random verification of our models, we have resorted to ensuring that the synthesized layouts actually perform as desired by comparison to finite element analysis and experimental measurements of fabricated devices.

The layout synthesis approach is outlined initially, followed by a discussion of the models and their derivation. We then describe the synthesis results, and verify our models via simulation and fabrication experiment.

SYNTHESIS APPROACH

The goal of layout synthesis is to find a "good" design which meets the design specifications. In order to achieve this goal, the synthesis is formulated as a non-linearly constrained optimization problem with the design mask geome-

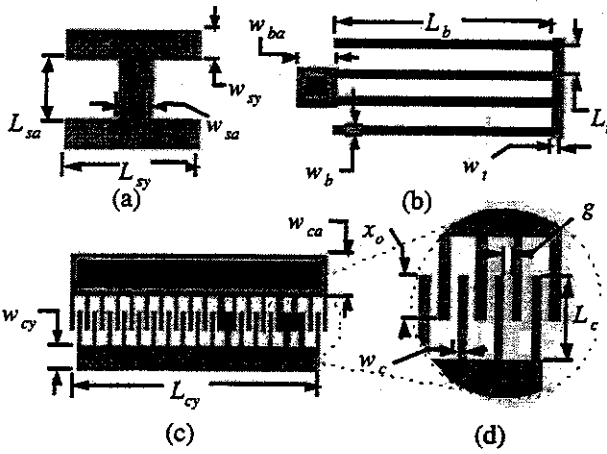


FIGURE 2. Parameterized microresonator elements. (a) shuttle mass, (b) folded flexure, (c) comb drive with N movable 'rotor' fingers, (d) close-up view of comb fingers.

try parameterized into design variables as shown in Figure 2. We now have to find a set of values for these design variables which minimize a design quality metric, such as, device area, and satisfy certain performance-ensuring constraints. The knowledge about the physics, geometry and processing is captured in these constraints as lumped-parameter models which are functions of the design variables.

The non-linear constrained optimization formulation can be written as:

$$\begin{aligned} \min_{\underline{u}} \quad & z = \sum_{i=1}^{\kappa} w_i \cdot f_i(\underline{u}) \\ \text{s.t.} \quad & h(\underline{u}) = 0 \\ & g(\underline{u}) \leq 0 \\ & \underline{u} \in U_P \end{aligned}$$

where \underline{u} is the vector of independent variables given in Table I; $f_i(\underline{u})$ is a set of objective functions that codify design quality metrics, e.g., area; $h(\underline{u}) = 0$ and $g(\underline{u}) \leq 0$ are each a set of functions that implement the geometric and functional constraints.

The geometric constraints limit the overall size of the resonator and also prevents the movable resonator shuttle from crashing into the stationary parts. These constraints can be written as mostly linear functions of the mask geometry variables.

The functional design constraints are listed in Table II. The resonant frequency constraint ensures that the user-specification on frequency (f_{spec}) is met. The next two constraints ensure that the resonator moves adequately at resonance and has a quality factor greater than 5, respectively. The two stability constraints are required to prevent the

Table I. Design variables for the microresonator. Upper and lower bounds are in units of μm except N and V .

var.	description	min.	max.
L_b	length of flexure beam	2	400
w_b	width of flexure beam	2	20
L_t	length of truss beam	2	400
w_t	width of truss beam	2	20
L_{sy}	length of shuttle yoke	2	400
w_{sy}	width of shuttle yoke	10	400
w_{sa}	width of shuttle axle	10	400
w_{cy}	width of comb yoke	10	400
L_{cy}	length of comb yoke	2	700
L_c	length of comb fingers	8	400
w_c	width of comb fingers	2	20
g	gap between comb fingers	2	20
x_o	comb-finger overlap	4	400
N	number of rotor comb fingers	1	100
V	voltage amplitude	1 V	50 V
w_{ba}	width of beam anchors	11	11
w_{ca}	width of stator comb anchors	14	14

moving comb fingers from snapping to the stationary comb fingers, due to an electrostatic imbalance force in the y -direction or an imbalance torque about z . The imbalance force and torque may be caused by small displacements away from the center (the equilibrium position), for example, due to manufacturing mismatch.

The mode decoupling constraints (there are seven of them) are necessary to ensure that the x -mode resonant frequency dominates. The three in-plane resonant frequencies

Table II. Functional Constraints.

Constraint Description	Expression	min	max
resonant frequency	f_x/f_{spec}	0.99	1.01
stroke at resonance	x_{disp}	2 μm	100 μm
quality factor	Q_x	5	10^5
y -axis stability	$k_{e,y}/k_y$	0	1/3
θ_z stability	$k_{e,\theta z}/k_{\theta z}$	0	1/3
in-plane mode decoupling	f_x/f_i	0	1/3
out-of-plane mode decoupling	f_x/f_o	0	1/2
k_y accuracy	$k_y/k_{y,axle}$	0	1/10
k_x accuracy	x_{disp}/L_b	0	1/10
buckling	L_y/L_{cr}	0	1/2

(f_i) are constrained to be at least thrice that of the x -mode while the out-of-plane resonant frequencies (f_o) are constrained to be at least twice that of the x -mode. These separations are sufficient to ensure that the secondary displacements are small enough so as not to couple with the primary displacement direction.

Since higher-order effects are not completely modeled, the synthesis is prevented from searching in those regions of the design space where they may be significant. This is achieved through the accuracy constraints. Finally, the beams are constrained to be shorter than the critical buckling length through the last constraint in Table II.

MODELING

Models required for synthesis include resonant frequencies of the oscillation modes, damping in the fundamental mode and the electrostatic comb-drive force.

Each oscillation is described by a lumped second-order equation of motion. For any generalized displacement ζ , we can write:

$$F_{e,\zeta} = m_\zeta \ddot{\zeta} + B_\zeta \dot{\zeta} + k_\zeta \zeta \quad (1)$$

where $F_{e,\zeta}$ is the external force (in the x -mode this force is generated by the comb drives), m_ζ is the effective mass, B_ζ is the damping coefficient, and k_ζ is the spring constant. Now, for example, the x -mode frequency is given by $\omega_x = 2\pi f_x = \sqrt{k_x/m_x}$. The other modes are modeled similarly.

Linear equations for the spring constants are derived using energy methods. A force (or moment) is applied to the free end(s) of the spring, in the direction of interest, and the displacement is calculated symbolically (as a function of the design variables and the applied force). In these calculations different boundary conditions are applied for the different modes of deformation of the spring.

When forces (moments) are applied at the end-points of the flexure, the total energy of deformation, U , is calculated as:

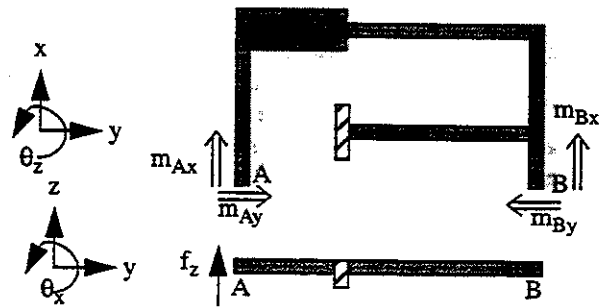
$$U = \sum_{\text{beam } i=1}^N \int_0^{L_i} \frac{M_i(\xi)^2}{2EI_i} d\xi \quad (2)$$

where, L_i is the length of the i 'th beam in the flexure, M_i is the bending moment transmitted through beam i , E is the Young's modulus of polysilicon and I_i is the moment of inertia of beam i , about the relevant axis. The bending moment is a linear function of the forces and moments applied to the end-points of the flexure. The displacement of an end-point of the flexure in any direction ζ is given as:

$$\delta\zeta = \frac{\partial U}{\partial F_\zeta} \quad (3)$$

where, F_ζ is the force applied in that direction at that end point [6]. Similarly, angular displacements can be related to applied moments.

Our aim here is to obtain the displacement in the direction of interest as a function of the applied force in that direction. Applying the boundary conditions, as shown in Figure 3, we obtain a set of linear equations in terms of the applied forces and moments, and the unknown displacement. Solving the set of equations yields a linear relationship between the displacement and applied force in the direction of interest. The constant of proportionality gives the spring constant as a function of the physical dimensions of the flexure.



$$\text{Calculation of } k_{\theta_x} \quad \begin{matrix} \delta z = 0 \\ \delta \theta_y = 0 \end{matrix}$$

$$\begin{matrix} \delta \theta_y = 0 \\ m_{tx} = 0 \end{matrix}$$

$$\text{Calculation of } k_{\theta_y} \quad \begin{matrix} \delta z = 0 \\ \delta \theta_x = 0 \end{matrix}$$

$$\begin{matrix} \delta \theta_x = 0 \\ m_{ty} = 0 \end{matrix}$$

FIGURE 3. Forces and moments applied on the free ends of a half folded-flexure (with y -axis of symmetry). Boundary conditions to calculate the spring constants in the two out-of-plane rotational modes are also shown.

The out-of-plane models for the spring constants and effective masses augment other similarly derived in-plane models and equations derived in [7], to form the complete set of mode-separation constraints used in the synthesis.

Viscous air damping dominates the energy dissipation mechanisms in microresonators in atmospheric pressure. The total damping force in the x -direction is mainly composed of the forces due to Couette flow below the resonator, Stokes flow above the resonator and air flow in the gap between comb-fingers. The expression for the damping coefficient is [8]:

$$B_x = \mu \left[(A_s + 0.5A_t + 0.5A_b) \left(\frac{1}{d} + \frac{1}{\delta} \right) + \frac{A_c}{g} \right] \quad (4)$$

where μ is the viscosity of air, d is the fixed spacer gap of $2 \mu\text{m}$, δ is the penetration depth of airflow above the structure, g is the gap between comb fingers, and A_s , A_t , A_b , and A_c are layout areas for the shuttle, truss beams, flexure beams, and comb-finger sidewalls, respectively. In order to take into account edge and finite-size effects, these areas are calculated after extending each length by $4 \mu\text{m}$. Damping factors of the other modes do not enter into the design constraints and are not calculated.

General analytic equations for the lateral comb-drive force, F_x , as a function of comb-finger width (w_c), g , structure thickness (t), and sacrificial spacer thickness (d) are derived in [10]. For the special case of equal comb-finger width, gap, thickness, and spacing above the substrate ($w_c = g = t = d$), each comb-drive generates a force that is proportional to the square of the voltage, V , applied across the comb fingers:

$$F_{e,x} \cong 1.12 \epsilon_0 N \frac{t}{g} V^2 \quad (5)$$

where ϵ_0 is the permittivity of air.

SYNTHESIS RESULTS

Previously, we have synthesized layouts which were optimized for different objective functions such as minimize microresonator area, minimize applied voltage, minimize a normalized sum of microresonator area and applied voltage and maximize microresonator displacement at resonance [5]. These resonators were fabricated in the MUMPS process [9]. All these devices are $2 \mu\text{m}$ thick. Representative layouts are shown in Figure 4 (a) and (b). After the incorporation of the out-of-plane mode-separation constraints in the synthesis tool, an attempt was made to synthesize layouts as before. However, it was found that the thickness of $2 \mu\text{m}$

was not sufficient to meet these new constraints. With higher structural thickness the springs would be stiffer in the out-of-plane modes and, therefore, these modes would have higher resonant frequencies. Hence, we introduced the structural thickness as a new design variable and implemented a new objective function: minimize a normalized sum of microresonator area, applied voltage and structural thickness. The layouts generated are shown in Figure 4(c). The thicknesses range from $3.7 \mu\text{m}$ to $9.1 \mu\text{m}$. The mode-separation constraints are more significant near the design corners, i.e., for the 300 KHz resonator. It is seen that the 300 KHz resonator in Figure 4 (b) has the least number of fingers and, therefore, has a smaller moment of inertia about the z-axis (pointing out of the plane of the paper). This is necessitated by the rotation-about-z mode separation constraint. On the other hand, the 300 KHz resonator in Figure 4(c) has more comb-fingers. However, since the design has a much thicker and wider truss beam, the mode-separation constraint can still be met even though the moment of inertia is relatively large.

VERIFICATION

The synthesized microresonators were simulated with FEA using 3D beam elements and the frequencies of the out-of-plane modes were compared to the frequencies predicted by the analytical models. As seen in Figure 6, the model for f_z is accurate to about 10% even at 100 KHz.

However, as seen in Figure 7 and Figure 8, the models for the out-of-plane rotational modes, f_{θ_x} and f_{θ_y} , are accurate only at lower frequencies. It is expected that, if second-order effects such as axial tension and shear stress are also considered, the models' accuracy can be improved.

In order to verify whether the mode-separation constraints were actually met, the first 5 modes of a newly syn-

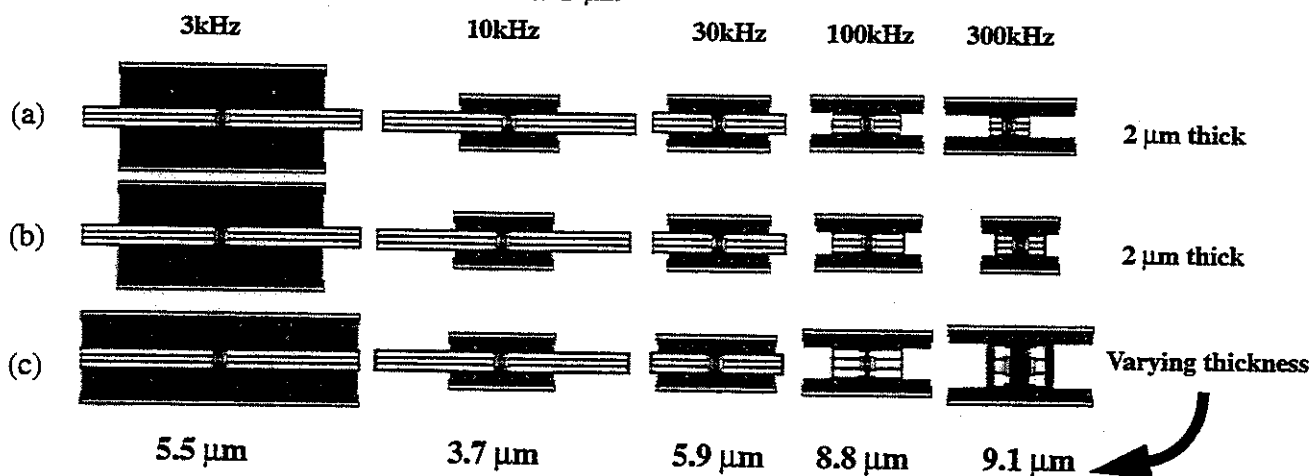


FIGURE 4. Comparison of layouts generated using increasing number of mode-separation constraints for five frequencies. (a) 1 mode-separation constraint (b) 3 in-plane mode-separation constraints (c) 3 in-plane and 4 out-of-plane mode-separation constraints. Layouts are optimized for area, voltage and thickness.

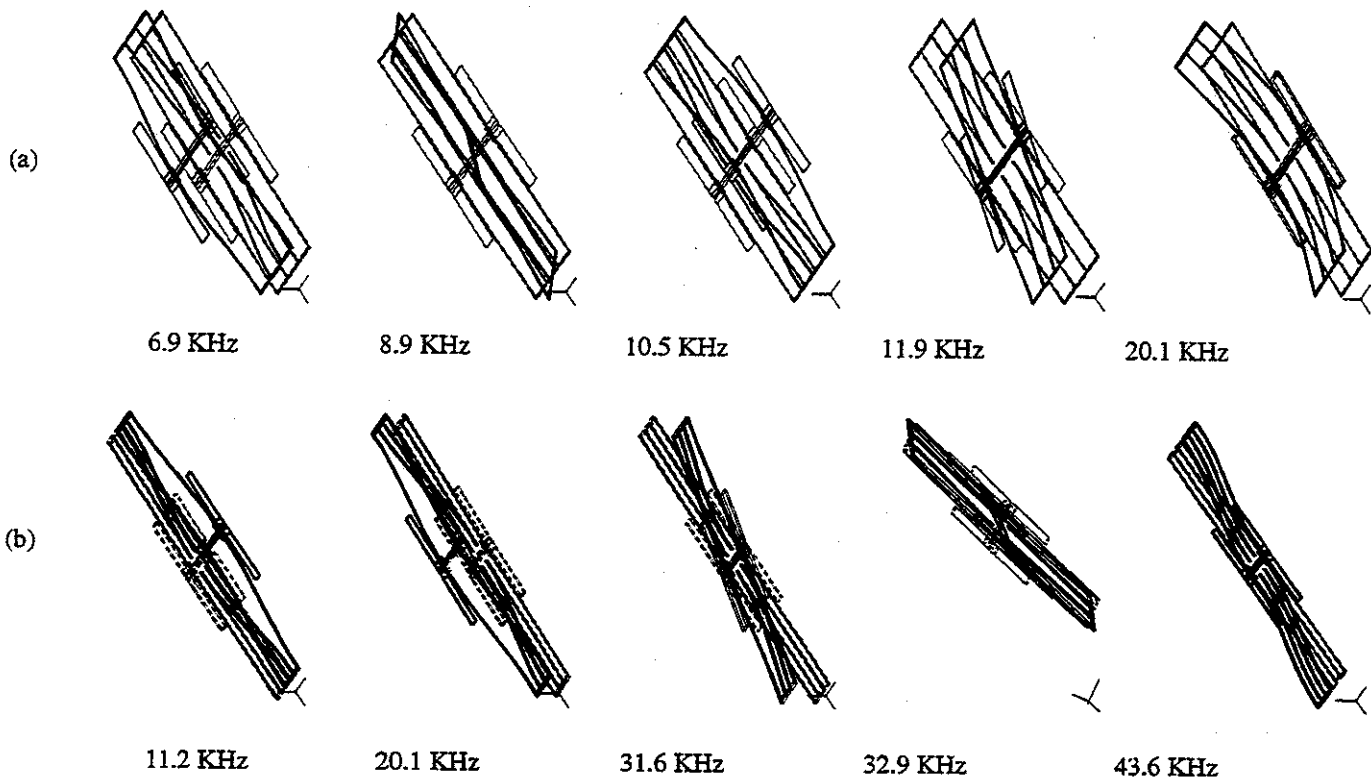


FIGURE 5. Simulated vibration modes of two 10 KHz resonators. (a) Modes for the resonator synthesized with the in-plane mode-separation constraints only. The dominant mode in this case is the z-translation mode at 6.9 KHz. (b) Modes for the resonator synthesized with the out-of-plane mode-separation constraints as well. The thickness of this resonator is $3.7\mu\text{m}$. The dominant mode is the preferred x-translation mode and all the other vibration modes are well-separated from the dominant mode.

thesized resonator were compared to those of a previously synthesized resonator of the same frequency.

As shown in Figure 5, the new resonators have the preferred x-translation mode as the lowest frequency mode.

EXPERIMENTAL VERIFICATION

Resonators were fabricated in MUMPS and the resonant frequency and the quality factor were measured. These

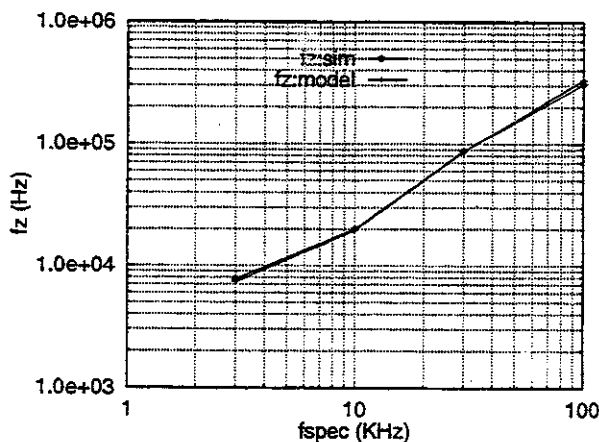


FIGURE 6. Comparison of model with FEM simulation (frequency of the z-translation mode) for resonators in Figure 4(c)

measured results were compared with analytical model results. The fabricated resonators were affected by beam over-etching, resulting in a trapezoidal cross-section with beam widths being smaller than the designed values. Models for trapezoidal cross-section were incorporated in the synthesis tool and the synthesized designs were evaluated taking measured over-etch parameters into account, for one-to-one verification with measured functional performance data. As seen in Figure 9, these analytical models are quite accu-

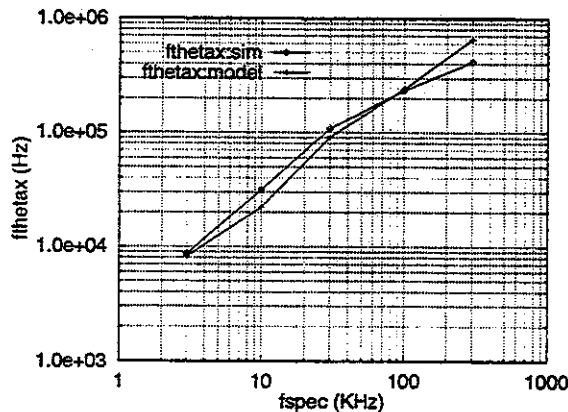


FIGURE 7. Comparison of model with FEM simulation (frequency of the rotation-about-x mode, $f_{\theta_{\text{ax}}}$) for resonators in Figure 4(c)

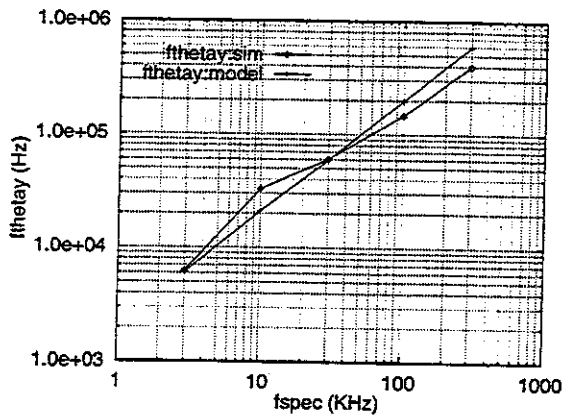


FIGURE 8. Comparison of model with FEM simulation (frequency of the rotation-about-y mode, f_{θ_y}) for resonators in Figure 4(c)

rate. The measured resonant frequency matches to within 4% of the model. This implies that, if we were to have a process that has a well-characterized over-etch, we would be able to synthesize layouts whose performance will be exactly as expected.

The quality factor is accurate to about 20% at high frequencies (at 20kHz, the model is accurate to within 5%). The quality factor model depends primarily on the damping models used. At higher frequencies, when the dimensions are small, the edge and finite-size damping effects become more significant. Hence, we see more error in the quality factor model at higher frequencies. We are currently using numerical simulation to understand the sources of damping at the different frequencies to discern the actual cause of inaccuracy.

CONCLUSIONS

Microresonators with well-controlled modes of oscillation have been synthesized. The models used can predict the frequencies for the out-of-plane modes with accuracies sufficient for synthesis purposes. We have shown that these out-of-plane modes are significant, and need to be considered during synthesis. The experimental measurements also

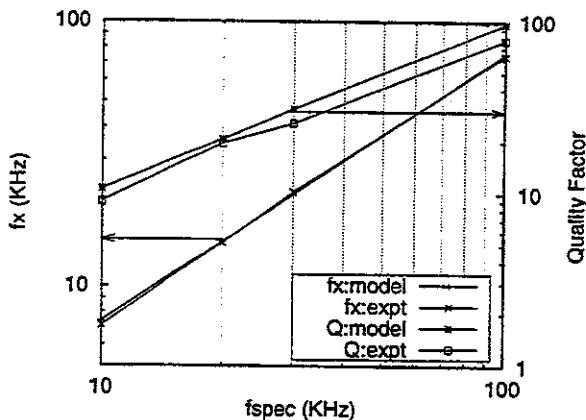


FIGURE 9. Comparison of measurements of resonant frequency and quality factor with models.

confirm that the models for spring stiffness, effective mass and damping in the preferred, x -mode of motion, are accurate. In order to extend the range of validity of models, higher order effects should be considered. With these extensions the approach described can be used effectively for rapid synthesis of suspended microstructures.

ACKNOWLEDGEMENTS

The authors thank Karen Markus and Ramaswamy Mahadevan of MCNC for use of the CaMEL tool and Hasnain Lakdawala for help with the measurements. This research effort is sponsored by the Defence Advanced Research Projects Agency (DARPA) and U. S. Air Force Research Laboratory, under agreement number F30602-96-2-0304. The U.S. Government is authorized to reproduce and distribute reprints for governmental purposes notwithstanding any copyright notation thereon. The views and conclusions contained herein are those of the authors and should not be interpreted as necessarily representing the official policies or endorsements, either expressed or implied, of DARPA, the U. S. Air Force Research Laboratory, or the U. S. Government.

REFERENCES

- [1] W. C. Tang, T.-C. H. Nguyen, M. W. Judy, and R. T. Howe, "Electrostatic Comb Drive of Lateral Polysilicon Resonators", *Sensors and Actuators A*, 21 (1990) 328-331.
- [2] *CaMEL Web Page*, <http://www.mcnc.org/camel.org>, MCNC MEMS Technology Applications Center, 3021 Cornwallis Road, Research Triangle Park, NC 27709.
- [3] N. R. Lo, E. C. Berg, S. R. Quakkelaar, J. N. Simon, M. Tachiki, H.-J. Lee, and K.S.J.Pister, "Parametrized layout synthesis, extraction, and SPICE simulation for MEMS," *Proc. ISCAS*, Atlanta, GA, 1996, pp. 481-484.
- [4] D. Haronian, "Maximizing microelectromechanical sensor and actuator sensitivity by optimizing geometry," *Sensors and Actuators A*, 50 (1995) 223-236.
- [5] G.K. Fedder and T. Mukherjee, "Automated Optimal Synthesis of Microresonators," *Proc. 9th Intl. Conf. on Solid-State Sensors and Actuators (Transducers '97)*, Chicago, IL, June 16-19, 1997.
- [6] J. M. Gere and S. P. Timoshenko, *Mechanics of Materials*, PWS Publishing Company, Boston, 4th edition, 1997.
- [7] G. K. Fedder, "Simulation of Microelectromechanical Systems", *Ph. D. Thesis*, Department of Electrical Engineering and Computer Sciences, University of California at Berkeley, September 1994.
- [8] X. Zhang and W. C. Tang, "Viscous Air Damping in Laterally Driven Microresonators," *Sensors and Materials*, v. 7, no. 6, 1995, pp.415-430.
- [9] D. A. Koester, R. Mahadevan, K. W. Markus, *Multi-User MEMS Processes (MUMPs) Introduction and Design Rules*, MCNC MEMS Technology Applications Center, 3021 Cornwallis Road, Research Triangle Park, NC 27709, rev. 3, Oct. 1994.
- [10] W. A. Johnson and L. K. Warne, "Electrophysics of Micro-mechanical Comb Actuators," *J. of Microelectromechanical Systems*, v.4, no.1, March 1995, pp.49-59.